Journal of Thermal Science Vol.28, No.5 (2019) 1042−1053

https://doi.org/10.1007/s11630-019-1202-9 **Article ID: 1003-2169(2019)05-1042-12**

Experimental Study on Thermal Performance of FLNG Spiral Wound Heat Exchanger under Sloshing Conditions

YAN Yan, SUN Chongzheng, HAN Hui, LI Yuxing*

College of Pipeline and Civil Engineering / Shandong Provincial Key Laboratory of Oil & Gas Storage and Transportation Safety / Qingdao Key Laboratory of Circle Sea Oil & Gas Storage and Transportation Technology, China University of Petroleum , Qingdao 266580, China

Abstract: The FLNG spiral wound heat exchanger (SWHE) is affected by the sea conditions, which leads to more complex flow process and decrease the heat transfer performance of the heat exchanger. In order to study the thermal performance of FLNG SWHE under heaving and swaying conditions, the experimental devices of FLNG SWHE and six-DOF (degree of freedom) sloshing platform were built. The effects of heaving and swaying motions on the pressure drop and heat transfer characteristics were analyzed at different sloshing amplitudes. The results showed that the heaving and swaying motions can cause the temperature rise and pressure fluctuation of SWHE, especially for swaying. The effect of sloshing on the heat transfer performance at the top of SWHE was greater than bottom. The pressure fluctuation percentage was within 7% and the amount of temperature change was less than 2°C, under the sloshing displacement among 120–255 mm.

Keywords: spiral wound heat exchanger, FLNG, experimental, sloshing

1. Introduction

In order to develop the offshore gas fields, a new type of floating production equipment named FLNG was built [1]. Many functions like natural gas extraction, loading and unloading, pre-treatment, liquefaction and storage are incorporated into FLNG. It can achieve greater economic efficiency by relocating to other gas fields [2,3]. The SWHEs are widely used in FLNG process to liquefy the natural gas, which have been fully analyzed under static state [4,5]. Neeraas et al. [6,7] and Hu et al. [8] developed heat transfer coefficient and pressure drop correlations for shell-side SWHE. Ding et al. [9,10] established an experimental rig to study the heat transfer performance of two-phase propane downward flow boiling in shell-side FLNG SWHEs. In order to improve the heat transfer performance of SWHE, Wang et al. [11,12] numerically studied the effects of geometrical parameters on thermal resistance of shell-side SWHEs. Jian et al. [13] numerically investigated the effects of major axis and minor axis of elliptical tubes on heat transfer performance of SWHE. Yu et al. [14] experimentally studied the two-phase heat transfer and frictional pressure drop performance of tube-side SWHE. In addition, Yu et al. [15,16] numerically studied the heat transfer coefficient of refrigerant mixtures in tube-side SWHE. Qiu et al. [17,18] numerically investigated the heat transfer coefficients of mixed hydrocarbon refrigerants in tube-side SWHE,

Received: Mar 31, 2019 AE: MA Weigang Corresponding author: LI Yuxing E-mail: liyx@upc.edu.cn

Nomenclature

A	area/m^2	We	Webb number
a	constant	x	dryness
Bo	boiling number	**Greek symbols**	
b	constant	α	heat transfer coefficient of SWHE/$W\cdot m^{-2}\cdot °C^{-1}$
c	constant	δ_c	film thickness/m
D	diameter/m	λ	thermal conductivity coefficient/$W\cdot m^{-2}\cdot °C^{-1}$
d	constant	μ	viscosity/Pa·s
g	gravitational acceleration/$m\cdot s^{-2}$	ρ	density/$kg\cdot m^{-3}$
M	molecular weight/$g\cdot mol^{-1}$	**Subscripts**	
Nu	Nusselt number	c	winding diameter
Pr	Prandtl number	h	equivalent diameter
Q	heat exchange/W	i	inner diameter
q	total heat flux/W	$LMTD$	log mean temperature difference
q_{sv}	pure-gas heat flux/W	l	thin-film tube-side SWHE
Re	Reynolds number	o	outer diameter
T	shell-side temperature/°C	s	shell-side SWHE
t	tube-side temperature/°C	sv	pure-gas tube-side SWHE
U	heat-transfer coefficient/$W\cdot m^{-2}\cdot °C^{-1}$	t	tube-side SWHE
u	flow velocity/$m\cdot s^{-1}$		

which indicated that the heat transfer coefficients varied largely with the increase of mass flow rate.

For predicting the dynamic performance of SWHEs under rolling conditions, a mathematical model of FLNG SWHE was proposed to describe the heat transfer relations among phase-change streams [19,20]. The comparison between the model prediction and experimental data showed that the model can predict the SWHE performance under the sloshing conditions well. Han et al. [21] numerically studied the falling film flow in shell-side SWHE under offshore conditions. Wang et al. [22] proposed a mathematical model of FLNG SWHEs under rolling conditions, which showed that the heat exchange performance decreased with the increase of the sloshing amplitude. Li et al. [23-26] numerically investigated the condensation characteristics in smooth and enhanced spiral pipes to improve the heat transfer performance of SWHE. Based on the former simulation model, Li et al. [27] investigated the heat transfer performance of S tube-side SWHE under sloshing conditions. The results showed that the effects of heaving motion on heat transfer performance were larger than that of other sloshing motions. Yu et al. [28] and Ren et al. [29,30] built a numerical simulation model to simulate the flow and heat transfer of shell-side SWHE under sloshing conditions, based on the FLUENT software. The results showed that the effects of pitching and heaving motions were much more significant than that of rolling.

Due to the lack of experimental research on the thermal performance of FLNG SWHE, the experimental devices of FLNG SWHE and six-DOF sloshing platform were built to study the effect of sloshing motion on the thermal performance of FLNG SWHE.

2. Experimental Apparatus

A flow diagram of the DMR (dual mixed refrigeration) liquefaction process is shown in Fig. 1, which consists of three circuits: feed gas circuit, pre-cooling circuit and test circuit. The compositions of feed gas, pre-cooling mixed refrigerant and cryogenic mixed refrigerant are shown in Tables 1, 2 and 3, respectively.

The experimental devices of FLNG SWHE was built and shown in Fig. 2. The FLNG SWHE was on the sloshing platform and connected to the feed gas circuit, pre-cooling circuit and test circuit via the low-temperature resistant hoses. The experimental uncertainties and parameters of FLNG SWHE are given in Tables 4 and 5.

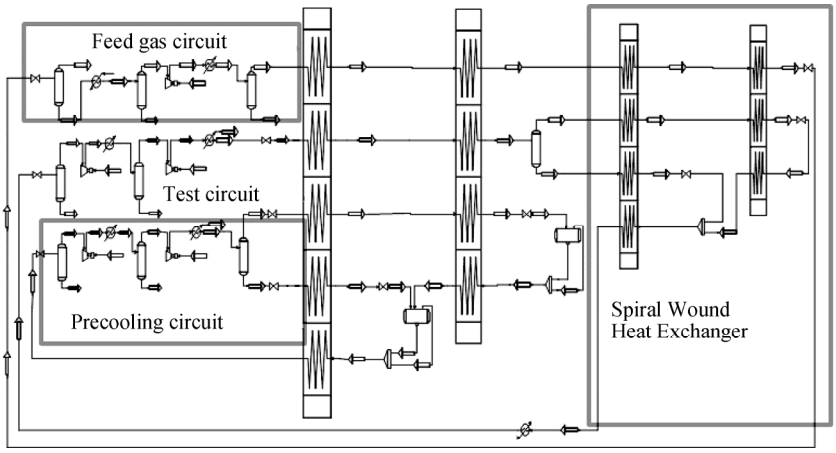

Fig. 1 Flowchart of DMR liquefaction process

Table 1 Composition of feed gas

Component	Fraction/%
Nitrogen	3.05
Methane	89.62
Ethane	0
Ethylene	5.83
Propane	0.14
Butane	1.36

Table 2 Composition of pre-cooling mixed refrigerant

Component	Fraction/%
Nitrogen	1.42
Methane	0.83
Ethane	2.06
Ethylene	29.46
Propane	63.13
Butane	3.09

Table 3 Composition of cryogenic mixed refrigerant

Component	Fraction/%
Nitrogen	8.21
Methane	20.25
Ethane	2.95
Ethylene	49.99
Propane	18.6
Butane	0

Fig. 2 Experimental device of FLNG SWHE

Table 4 Uncertainties

Instruments	Uncertainty
Pressure	±0.075%
Temperature	±0.1°C
Mass flow rate	±0.35%

Table 5 Parameters of FLNG SWHE

Item	Value
Internal diameter/mm	3.0
Thickness of pipeline/mm	0.5
Gas-phase pipeline length/m	47.0
Feed gas pipeline length/m	63.0
Liquid-phase pipeline length/m	55.0

3. Mathematical Model

The flow diagram of SWHE is shown in Fig. 3, which consists of the feed gas, tube-side and shell-side mixed refrigerant of SWHE.

The heat transfer performance of SWHE under sloshing conditions was analyzed by log mean temperature difference (*LMTD*) method.

$$\mathrm{Q} = UA \cdot \Delta T_{LMTD} \tag{1}$$

where ΔT_{LMTD} is:

$$\Delta T_{LMTD} = \frac{|T_1 - t_2| - |T_2 - t_1|}{\ln\left(\frac{T_1 - t_2}{T_2 - t_1}\right)} \tag{2}$$

The total heat exchange coefficient U is:

$$\frac{1}{U} = \frac{1}{\alpha_\mathrm{t}} \cdot \frac{D_\mathrm{o}}{D_\mathrm{i}} + \frac{D_\mathrm{o}}{2 \cdot \lambda} \cdot \ln\frac{D_\mathrm{o}}{D_\mathrm{i}} + \frac{1}{\alpha_\mathrm{s}} \tag{3}$$

where, T is the shell-side temperature, °C; t is the tube-side temperature, °C; A is the area, m^2; α_t is the tube side heat transfer coefficient, $\mathrm{W/(m^2 \cdot °C)}$; D_o is the

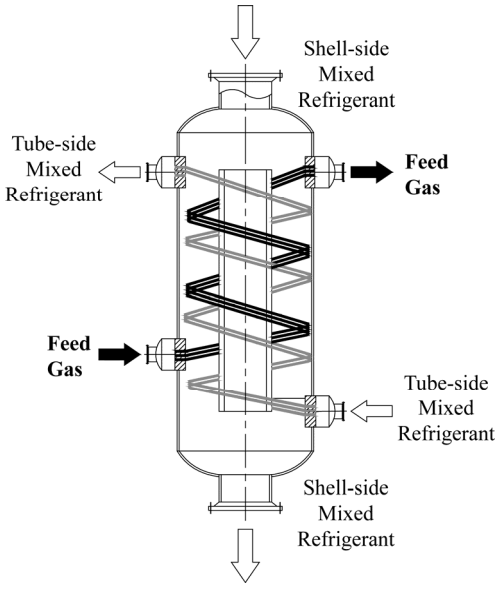

Fig. 3 Flow diagram of SWHE

external diameter of winding tube, m; D_i is the internal diameter of winding tube, m; λ is the thermal conductivity of tube wall, W/(m^2·°C); α_s is the shell side heat transfer coefficient, W/(m^2·°C)).

The calculation models of heat transfer coefficients of SWHE are given in Table 6. The single-phase and falling film shell-side heat transfer correlation applied on the FLNG SWHE has been verified in Refs. [6,7]. The results showed that heat transfer correlation agreed with the experimental data within the deviation of ±15%.

The two-phase shell-side heat transfer correlation applied on the LNG SWHE has been verified in Refs. [8, 10]. The results showed that heat transfer correlation agreed with 98% of the experimental data within the deviation of ±20%.

The tube-side heat transfer correlation applied on the LNG SWHE has been verified in Refs. [33,34]. The results showed that heat transfer correlation agreed with the experimental data within the deviation of ±12%.

Table 6 Heat transfer correlations of SWHE

Applied region	Correlations
Single-phase shell-side SWHE [31]	$Re<10000, Nu=0.6Re^{0.5}\cdot Pr^{0.31}$ $Re\geq 10000, Nu=0.36Re^{0.55}\cdot Pr^{0.33}\left(\frac{\mu}{\mu_w}\right)^{0.14}$, $\alpha_s=\frac{\lambda}{D_o}Nu$
Two-phase shell-side SWHE [8, 10]	$\alpha_s=S\cdot\alpha_{nb}+E\cdot\alpha_{cv}$ $\alpha_{cv}=0.039\cdot\lambda_l\cdot\left(\frac{v^2}{g}\right)^{-1/3}\cdot Re^{0.09}\cdot Pr^{0.99}$ $\alpha_{nb}=55\cdot Pr^{0.12-0.4343\ln Rp}\cdot(-0.4343\cdot\ln Pr)^{-0.55}\cdot M^{-0.5}\cdot q^{0.67}$ $Pr=P/P_{crit}$ $E=1+a_1\cdot(\phi^2)^{a2}\cdot Re^{a3}$ $S=b_1\cdot We^{b2}\cdot Bo^{b3}\cdot Pr^{b4}$
Falling film shell-side SWHE [6, 7]	$Nu=a\cdot\left(\frac{D_o}{\delta_c}\right)^c\cdot Re^b\cdot Pr^d$ $\delta_c=\left[\frac{\mu^2}{g\cdot\rho^2}\right]^{1/3}$ $\alpha_s=\frac{\lambda}{\delta_c}Nu$
Single-phase tube-side SWHE [31,33,34]	$100<Re<Re_c, \alpha_t=\left\{3.65+0.08\left[1+0.8\left(\frac{D_i}{D_c}\right)^{0.9}\right]Re^t\cdot Pr^{\frac{1}{3}}\right\}\frac{\lambda_i}{D_i}$, $t=0.5+0.2903\cdot\left(\frac{D_i}{D_c}\right)^{0.194}$ $Re_c<Re<2200, \alpha_t=\left\{0.023\left[1+14.8\left(1+\frac{D_i}{D_c}\right)\left(\frac{D_i}{D_c}\right)^{\frac{1}{3}}\right]Re^t\cdot Pr^{\frac{1}{3}}\right\}\frac{\lambda_i}{D_i}$, $t=0.8-0.22\cdot\left(\frac{D_i}{D_c}\right)^{0.1}$ $2200<Re<150000, \alpha_t=\left\{0.023\left[1+3.6\left(1-\frac{D_i}{D_c}\right)\left(\frac{D_i}{D_c}\right)^{0.8}\right]Re^t\cdot Pr^{\frac{1}{3}}\right\}\frac{\lambda_i}{D_i}$, $t=0.8$, $(Re)_c=2300\left[1+8.6(D_i/D_c)^{0.45}\right]$
Two-phase tube-side SWHE [32-34]	$\frac{1}{\alpha_t}=\frac{1}{\alpha_l}+\frac{q_{sv}/q}{\alpha_{sv}}$

Note: Please refer to these references for definition of the variables in Table 6.

Based on the heat transfer methods of Table 6, measured and calculated shell-side temperatures under swaying and heaving conditions are given in Table 7. The agreement between the calculated and measured data is better than ±8% for all data.

Table 7 Measured and calculated shell-side temperatures under swaying and heaving conditions

	Under swaying condition		Under heaving condition	
	Before	After	Before	After
Measured data/°C	-99.6	-98.6	-98.3	-97.6
Calculated data/°C	-94.15	-92.92	-90.47	-90.08
Deviation/%	5.47	5.76	7.97	7.70

4. Results and Discussion

4.1 Pressures and temperatures of SWHE under sloshing conditions

The experimental results of pressures and temperatures of SWHE under swaying and heaving conditions are shown in Figs. 4-11. The results show that sloshing motions led to the pressure fluctuation and increased the temperatures of SWHE, especially for swaying.

From Fig. 4, under the swaying displacement of 255 mm and the swaying period of 10 s, the tube-side gas-phase outlet pressure fluctuation is 0.015 MPa and the fluctuation amplitude percentage is 1.55%. The shell-side inlet pressure fluctuation value is 0.008 MPa and the fluctuation amplitude percentage is 6.71%. The tube-side inlet pressure and liquid-phase outlet pressure don't fluctuate under sloshing conditions. The tube-side gas-phase mixed refrigerant temperature increases to −120.29°C from −120.58°C. The feed gas temperature increases to −115.12°C from −116.58°C. This is because the swaying motion gives a horizontal velocity to the SWHE, which leads to the relative movement between the refrigerant and the tube wall. The uneven distribution of the refrigerant and feed gas leads to the pressure fluctuations and decreases the heat transfer performance of SWHE.

As shown in Fig. 5, under the swaying displacement of 190 mm and the swaying period of 10 s, the gas-phase tube-side outlet pressure fluctuation is 0.017 MPa and the fluctuation amplitude percentage is 1.83%. The shell-side inlet pressure fluctuation value is 0.008 MPa and the fluctuation amplitude percentage is 6.27%. The tube-side gas-phase mixed refrigerant temperature increases to −121.07°C from −121.56°C. The feed gas temperature increases to −116.58°C from −116.77°C.

From Figs. 6 and 7, under the swaying displacements of 155 mm and 120 mm, the tube-side gas-phase outlet pressure fluctuation amplitude percentages are 1.32% and 1.14% and the shell-side inlet pressure fluctuation amplitude percentages are 4.22% and 3.07%, respectively. The tube-side gas-phase mixed refrigerant temperature increases to −126.64°C from −126.93°C, for the swaying displacement of 155 mm. The tube-side gas-phase temperature increases to −121.85°C from −121.95°C, for the displacement of 120 mm. The feed gas temperatures both maintain stable.

From Fig. 8, under the heaving displacement of 255 mm and the heaving period of 10 s, the tube-side gas-phase outlet pressure fluctuation is 0.029 MPa and the fluctuation amplitude percentage is 2.96%. The pressure fluctuation period is different from the heaving period. The tube-side inlet pressure, liquid-phase outlet pressure and shell-side pressure don't fluctuate under sloshing conditions. The tube-side gas-phase mixed refrigerant temperature increases to −121.95°C from −122.93°C. The feed gas temperature increases to −119.19°C from −120.51°C. This is because the swaying motion gives a vertical velocity to the SWHE, which leads to the pressure fluctuation and decreases the heat transfer performance of SWHE.

As shown in Fig. 9, under the heaving displacement of 190 mm and the heaving period of 10 s, the tube-side gas-phase outlet pressure fluctuation is 0.017 MPa and

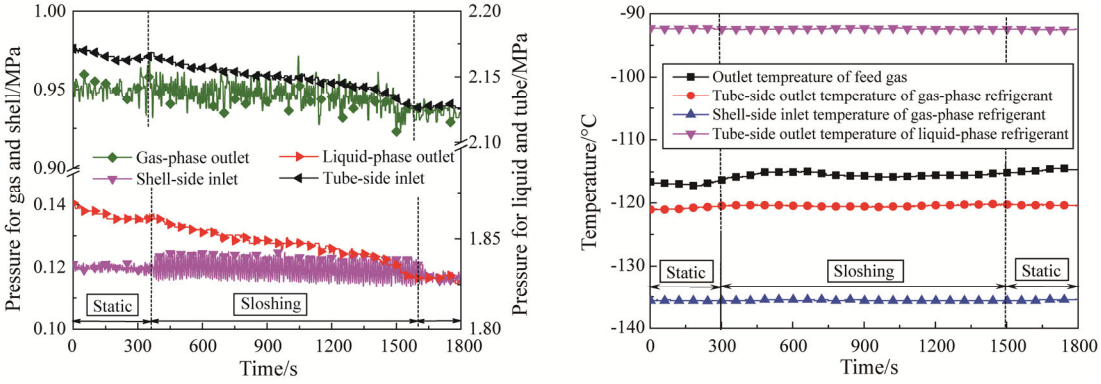

Fig. 4 Pressures and temperatures of SWHE under swaying condition (255 mm)

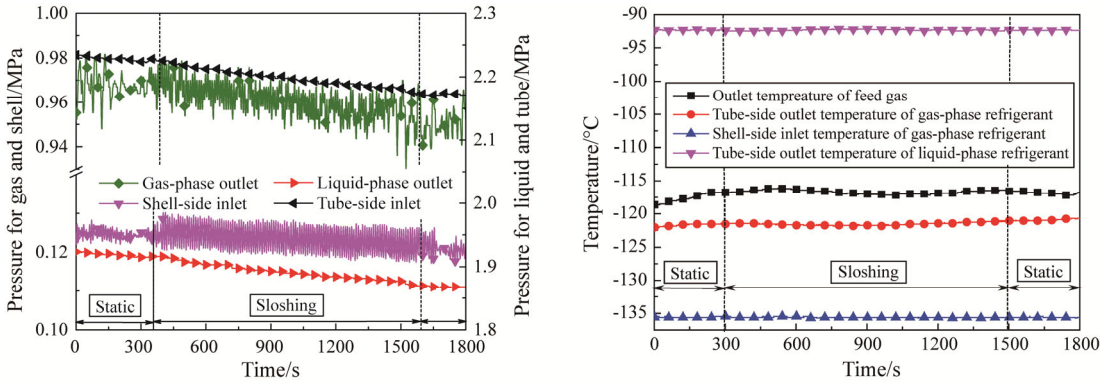

Fig. 5 Pressures and temperatures of SWHE under swaying condition (190 mm)

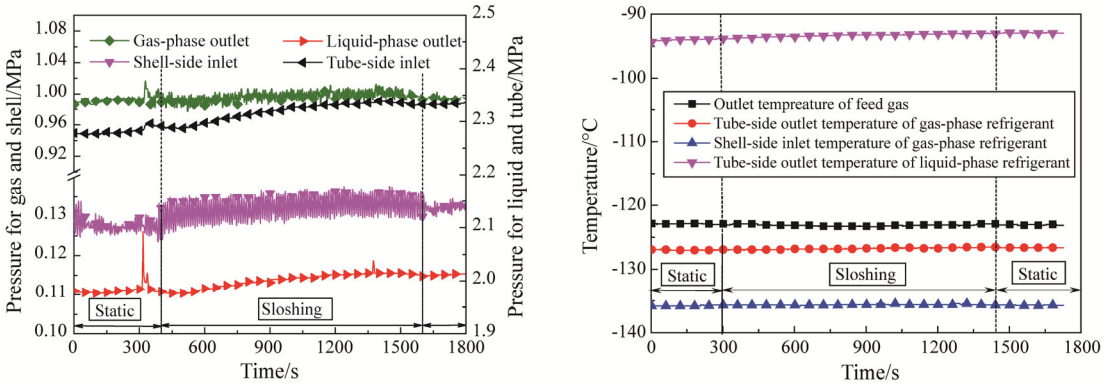

Fig. 6 Pressures and temperatures of SWHE under swaying condition (155 mm)

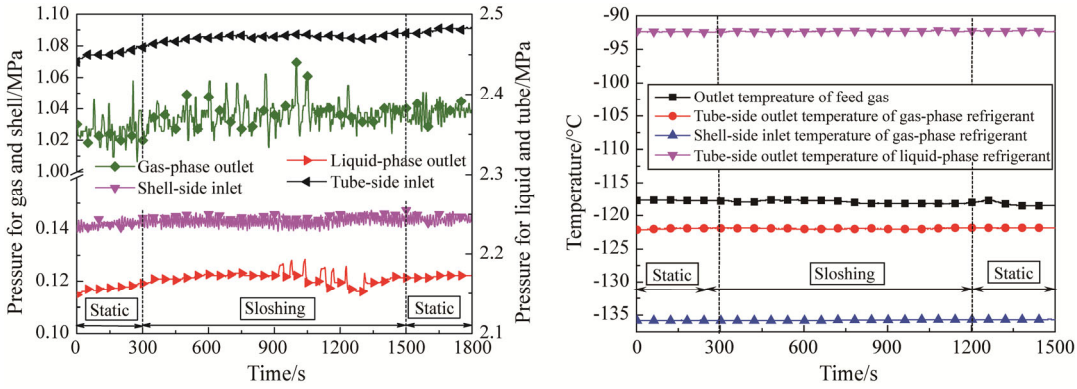

Fig. 7 Pressures and temperatures of SWHE under swaying condition (120 mm)

the fluctuation amplitude percentage is 1.75%. The tube-side gas-phase mixed refrigerant temperature increases to −123.71°C from −124.98°C. The feed gas temperature maintains stable.

From Figs. 10 and 11, under the heaving displacements of 155 mm and 120 mm, the heaving motion has little effect on the pressures of SWHE. The temperatures of tube-side gas-phase mixed refrigerant and feed gas increase to −128.69°C and −125.35°C from −129.28°C and −126.22°C respectively, for the heaving displacement of 120 mm.

4.2 *LMTD* of SWHE under sloshing conditions

LMTD is integral average of temperature difference between cold and hot fluid in the heat exchanger, which is one of the important parameters to investigate SWHE heat transfer performance. Under sloshing conditions, *LMTD* of SWHE changing over time is shown in Fig. 12.

Fig. 12 shows that under different amplitudes of oscillation, sloshing motions have the similar influence on heat transfer performance of SWHE, which is classified into three regions: quasi-steady region, intermediate region and performance deterioration region.

(1) In quasi-steady region, SWHE is under sloshing conditions, whose technological parameters are all in a static state, due to temperature hysteresis. Quasi-steady region is relatively short.

(2) In intermediate region, technological parameters of SWHE fluctuate dramatically, but still in the scope of design, because of its own sloshing resistance.

(3) After 800 s, as well as 500 sunder sloshing conditions, SWHE is in performance deterioration region, where offshore adaptability of SWHE is becoming poor, resulting in rapid increase of log mean temperature difference and deterioration of heat transfer performance.

4.3 Heat transfer performance of SWHE under sloshing conditions

Base on the experimental data and mathematical models of Eqs. (1)-(3) and Table 6, the calculated results

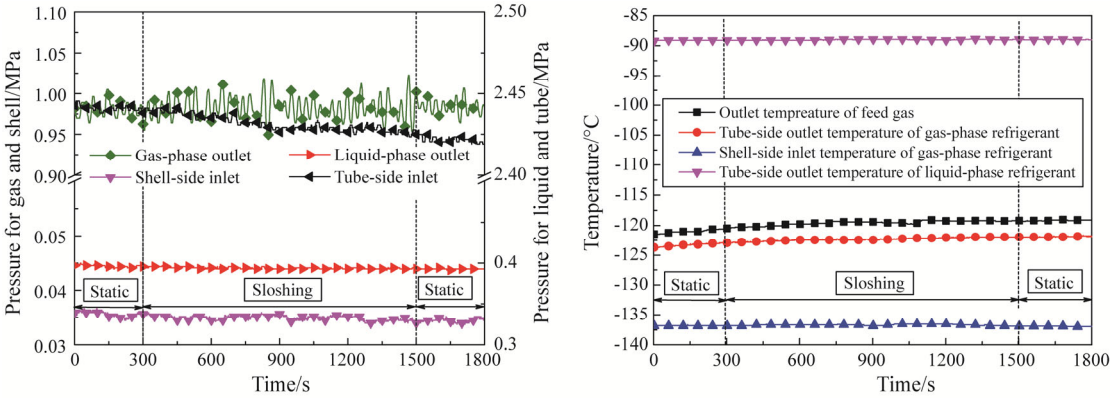

Fig. 8 Pressures and temperatures of SWHE under heaving condition (225 mm)

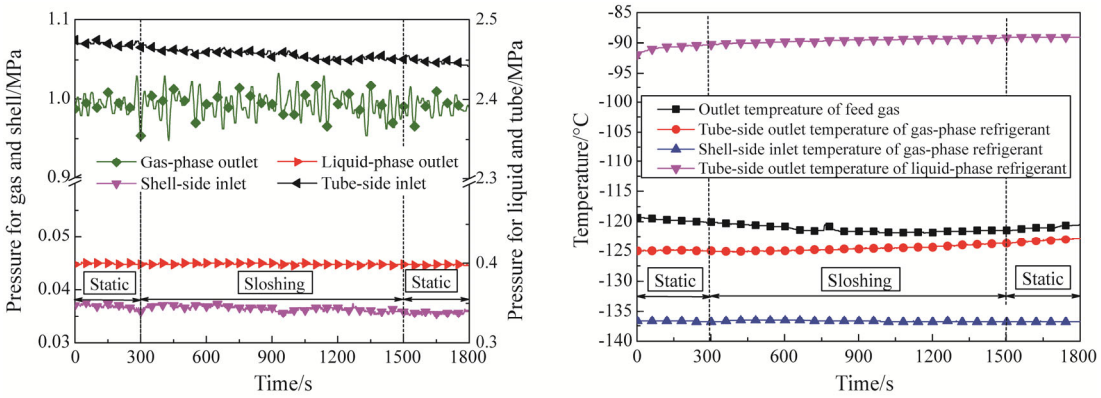

Fig. 9 Pressures and temperatures of SWHE under heaving condition (190 mm)

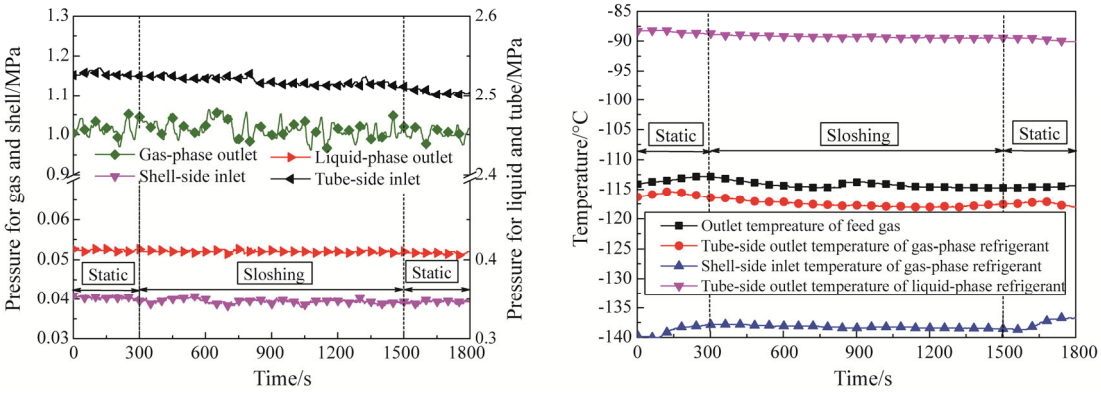

Fig. 10 Pressures and temperatures of SWHE under heaving condition (155 mm)

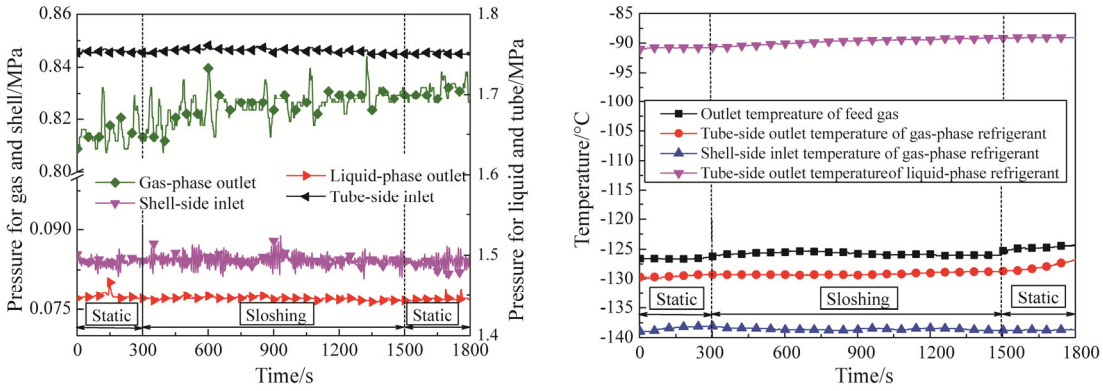

Fig. 11 Pressures and temperatures of SWHE under heaving condition (120 mm)

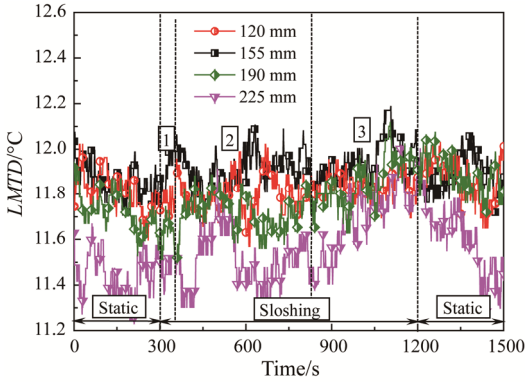

1. Quasi-steady region; 2. Intermediate region; 3. Performance deterioration region

Fig. 12 *LMTD* of SWHE under swaying condition

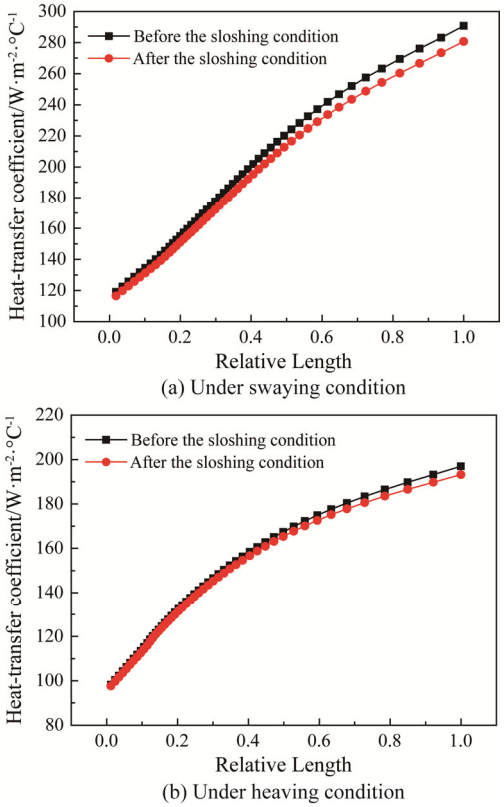

Fig. 13 Shell-side heat transfer coefficient of SWHE under swaying and heaving conditions

of temperature and heat transfer coefficient distribution of SWHE under swaying and heaving conditions are shown in Figs. 13, 14 and 15.

As shown in Fig. 13, the heat transfer coefficients of shell-side mixed refrigerant increase to 290.70 and 280.73 W/(m^2·°C) from 119.11 and 116.54 W/(m^2·°C) before and after the swaying condition, respectively. The heat transfer coefficients of shell-side mixed refrigerant increase to 196.97 and 193.19 W/(m^2·°C) from 98.18 and 97.61 W/(m^2·°C) before and after the heaving condition, respectively. It can be concluded that the heat transfer coefficient of the shell-side SWHE increases from bottom to top. This is because the shell-side cooling capacity of the SWHE applied on the DMR liquefaction process is mainly based on the latent heat of the liquid-phase mixed refrigerant. With the higher position, the liquid fraction of mixed refrigerant is higher and the latent heat is larger.

Under swaying and heaving condition, the shell-side heat transfer coefficients at the bottom of the SWHE decrease by 2.57 and 0.57 W/(m^2·°C), respectively. The shell-side heat transfer coefficients at the top of the SWHE decrease by 9.97 and 3.78 W/(m^2·°C), respectively. The effect of sloshing on the heat transfer performance at the top of SWHE is greater than the bottom. This is because falling film evaporation is a dominant heat transfer technology at the top of SWHE, which is highly susceptible to the sloshing motion. The shell-side mixed refrigerant is dominated by the gas phase at the bottom of the SWHE, and the sloshing motion has little effect on the gas-phase mixed refrigerant.

As shown in Fig. 14(a) and (b), under static condition, the heat exchange coefficients of feed gas, gas-phase and liquid-phase mixed refrigerant increase to 254.68, 262.85 and 268.61 W/(m^2·°C) from 110.82, 112.35 and 116.05

W/(m^2·°C), respectively. After swaying condition, the heat exchange coefficients of feed gas, gas-phase and liquid-phase mixed refrigerant increase to 244.92, 255.08 and 259.72 W/(m^2·°C) from 108.26, 109.76 and 113.59 W/(m^2·°C), respectively. It can be concluded that the heat exchange coefficient of liquid-phase mixed refrigerant is the largest, followed by the gas-phase mixed refrigerant and feed gas. This is because the flow rate of the liquid-phase mixed refrigerant is the largest compared to the feed gas and gas-phase mixed refrigerant. With the same pipe diameter (4 mm), the Reynolds number is large, resulting in a larger heat exchange coefficient.

As shown in Fig. 14(c) and (d), before heaving condition, the heat exchange coefficients of feed gas, gas-phase and liquid-phase mixed refrigerant increase to 177.80, 179.57 and 185.18 W/(m^2·°C) from 91.94, 92.19 and 95.59 W/(m^2·°C), respectively. After heaving condition, the heat exchange coefficients of feed gas, gas-phase and liquid-phase mixed refrigerant increase to 174.98, 177.40 and 181.50 W/(m^2·°C) from 91.49, 92.07 and 95.03 W/(m^2·°C), respectively. Similar to the shell-side heat transfer coefficient, the effect of sloshing on the tube-side heat exchange coefficient at the top of SWHE is greater than the bottom.

The sloshing effects on the heat transfer performance of SWHE are given in Table 8. It can be concluded that the swaying motion has a larger effect on the thermal performance of FLNG SWHE than heaving.

As shown in Fig. 15, the feed gas temperatures decrease to −91.63 and −89.07°C (−89.07°C = −89.07 + 273.15 K=184.08 K) from −39.44 and −35.36°C before and after swaying condition, respectively. The feed gas temperatures decrease to −91.38 and −87.37°C from −38.77 and −36.59°C before and after heaving condition, respectively. It can be concluded that the temperature drop rate of the tube-side feed gas decreases in the SWHE. This is because the inlet feed gas is pure gas phase, the absorbed cooling capacity of which is used to lower the temperature. The temperature drops faster. However, when the tube-side feed gas starts to be liquefied, most of the absorbed cooling capacity is used for the latent heat and the temperature drops slowly.

From Fig. 15, sloshing motions increase the temperatures of tube-side gas-phase mixed refrigerant. Under swaying and heaving conditions, the maximum temperature differences of gas-phase mixed refrigerant at the same location of SWHE are 2.16 and 1.76°C, respectively. The inlet gas-phase mixed refrigerant temperature drops faster than the liquid-phase mixed refrigerant. In the middle of SWHE, the gas-phase mixed refrigerant

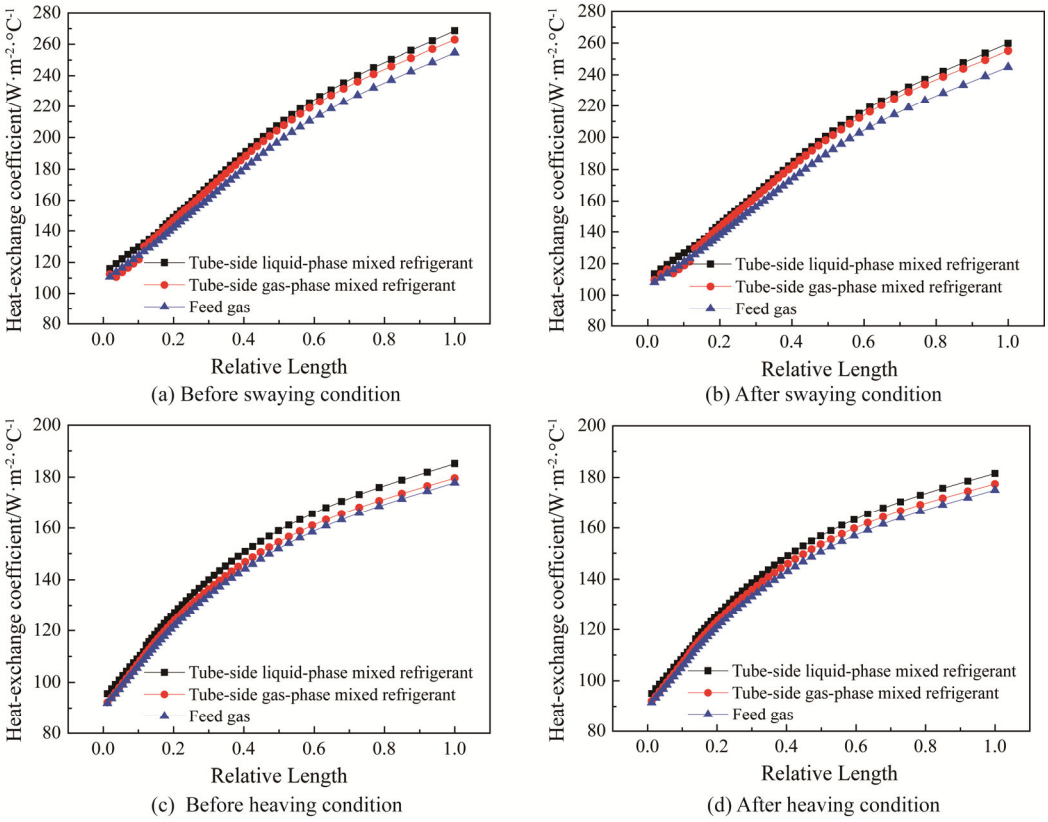

Fig. 14 Heat exchange coefficients of SWHE under swaying and heaving conditions

Table 8 Changing rates of heat transfer performance under swaying and heaving conditions

Position	Under swaying condition		Under heaving condition	
	Top	Bottom	Top	Bottom
Shell side	3.43%	2.16%	1.92%	0.58%
Gas phase	2.96%	2.30%	1.21%	0.13%
Liquid phase	3.31%	2.12%	1.99%	0.59%
Feed gas	3.83%	2.31%	1.59%	0.49%

temperature drop rate is lower than the liquid-phase mixed refrigerant. This is because the gas-phase mixed refrigerant flow rate is much lower than the liquid-phase mixed refrigerant. The temperature drop rate is faster at the bottom. As the temperature decreases, the gas-phase mixed refrigerant is gradually liquefied. The cooling capacity is mostly used for the latent heat of gas-phase mixed refrigerant. Therefore, the temperature drop rate is slower and gradually surpassed by the liquid-phase mixed refrigerant.

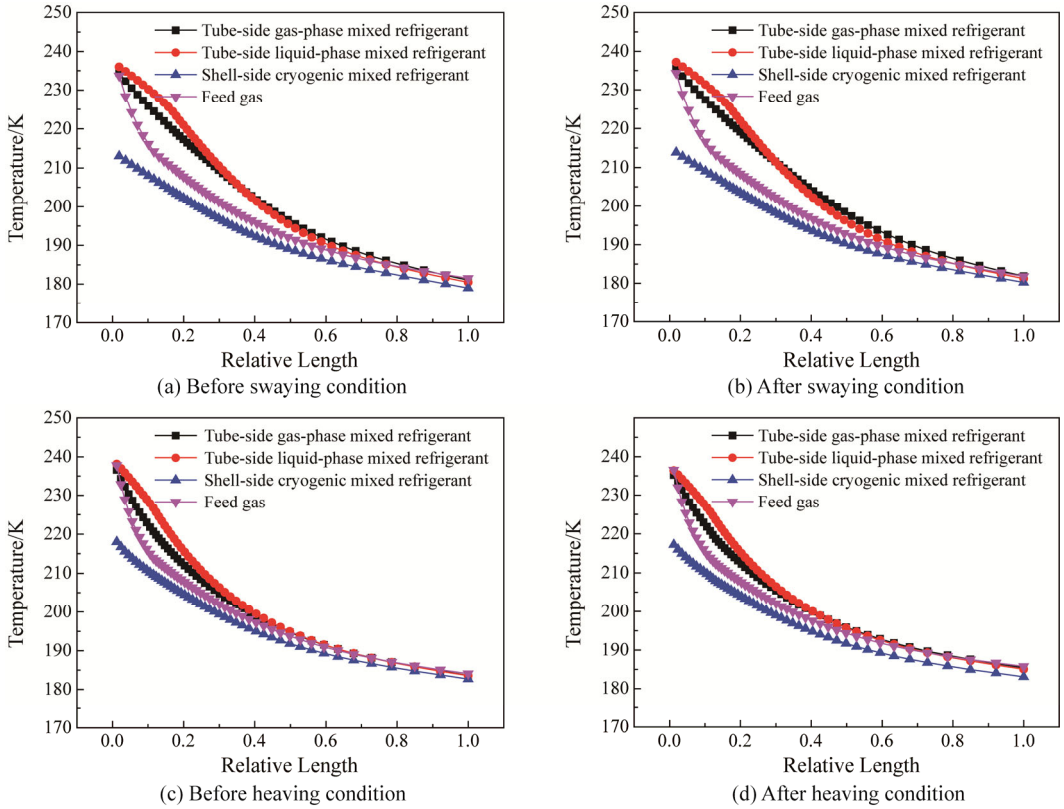

Fig. 15 Temperatures of SWHE under swaying and heaving conditions

4. Conclusions

The experimental devices of FLNG SWHE and six-DOF sloshing platform were built to understand the thermal performance of FLNG SWHE under sloshing conditions. Following conclusions are given:

(1) The sloshing motions can cause the temperature rise and pressure fluctuation of SWHE, especially for swaying. Under the sloshing displacement among 120−255 mm, the pressure fluctuation percentage was within 7% and the amount of temperature change was less than 2°C.

(2) Heat transfer performance of SWHE under sloshing conditions can be classified into three regions: quasi-steady region, intermediate region and performance deterioration region.

(3) The heat exchange coefficient of liquid-phase mixed refrigerant was the largest, followed by the gas-phase mixed refrigerant and feed gas. The heat transfer coefficient and effect of sloshing on the heat transfer performance at the top of SWHE were both larger than those at the bottom. At the top of the SWHE, the shell-side heat transfer coefficients decreased by 9.97 and 3.78 W/(m^2·°C) under swaying and heaving conditions, respectively.

Acknowledgements

The present work is supported by the National Natural Science Foundation of China (No. 51604294) and the Natural Science Foundation of Shandong Province of China (No. ZR2016EEQ02).

References

[1] Floating liquefied natural gas. http://en.wikipedia.org/wiki/Floating_liquefied_ natural_gas, 2003 (accessed on May 3, 2018).

[2] White G., Weiss C., Huguet E., Magne-Drisch J., Alix P., How waves can significantly impact performance of Amine unit installed on a FLNG? Houston: Offshore Technology Conference. 2014: 1–11.

[3] Sun C.Z., Li Y.X., Zhu J.L., et al., Experimental tube-side pressure drop characteristics of FLNG spiral wound heat exchanger under sloshing conditions. Experimental Thermal and Fluid Science, 2017, 88: 194–201.

[4] Li S., Cai W., Chen J., Zhang H., Jiang Y., Numerical study on the flow and heat transfer characteristics of forced convective condensation with propane in a spiral pipe. International Journal of Heat and Mass Transfer, 2018, 117: 1169–1187.

[5] Yu J., Jiang Y., Cai W., Li F., Forced convective condensation flow and heat transfer characteristics of hydrocarbon mixtures refrigerant in helically coiled tubes. International Journal of Heat and Mass Transfer, 2018, 124: 646–654.

[6] Bengt O., Arne O., Bjørn A., Experimental shell-side heat transfer and pressure drop in gas flow for spiral-wound LNG heat exchanger. International Journal of Heat and Mass Transfer, 2002, 47: 353–361.

[7] Bengt O., Arne O., Bjørn A., Experimental data and model for heat transfer, in liquid falling film flow on shell-side, for spiral-wound LNG heat exchanger. International Journal of Heat and Mass Transfer, 2004, 47: 3565–3572.

[8] Hu H.T., Ding C., Ding G.L., Heat transfer characteristics of two-phase mixed hydrocarbon refrigerants flow boiling in shell side of LNG spiral wound heat exchanger. International Journal of Heat and Mass Transfer, 2019, 131: 611–622.

[9] Ding C., Hu H.T., Ding G.L., Influences of tube pitches on heat transfer and pressure drop characteristics of two-phase propane flow boiling in shell side of LNG spiral wound heat exchanger. Applied Thermal Engineering, 2018, 131: 270–283.

[10] Ding C., Hu H.T., Ding G.L., Experimental investigation on downward flow boiling heat transfer characteristics of propane in shell side of LNG spiral wound heat exchanger. International Journal of Refrigeration, 2017, 84: 13–25.

[11] Wang S.M., Jian G.P., Xiao J., Fluid-thermal-structural analysis and structural optimization of spiral wound heat exchanger. International Communications in Heat and Mass Transfer, 2018, 95: 42–52.

[12] Wang S.M., Jian G.P., Wang J.R., Application of entransy-dissipation-based thermal resistance for performance optimization of spiral-wound heat exchanger. International Journal of Heat and Mass Transfer, 2018, 116: 743–750.

[13] Jian G.P., Wang S.M., Sun L.J., Numerical investigation on the application of elliptical tubes in a spiral-wound heat exchanger used in LNG plant. International Journal of Heat and Mass Transfer, 2019, 130: 333–341.

[14] Yu J.W., Chen J., Li F.Z., et al., Experimental investigation of forced convective condensation heat transfer of hydrocarbon refrigerant in a helical tube. Applied Thermal Engineering, 2018, 129: 1634–1644.

[15] Yu J.W., Jiang Y.Q., Cai W.H., et al., Numerical investigation on flow condensation of zeotropic hydrocarbon mixtures in a helically coiled tube. Applied Thermal Engineering, 2018, 134: 322–332.

[16] Yu J.W., Jiang Y.Q., Cai W.H., et al., Heat transfer characteristics of hydrocarbon mixtures refrigerant during condensation in a helical tube. International Journal of Thermal Sciences, 2018, 133: 196–205.

[17] Qiu G.D., Xu Z.F., Cai W.H., et al., Numerical study on the condensation flow and heat transfer characteristics of hydrocarbon mixtures inside the tubes of liquefied natural gas coil-wound heat exchangers. Applied Thermal Engineering, 2018, 140: 775–786.

[18] Qiu G.D., Wei X.H., Cai W.H., et al., Development and validation of numerical model of condensation heat transfer and frictional pressure drop in a circular tube. Applied Thermal Engineering, 2018, 143: 225–235.

[19] Duan Z.D., Ren T., Ding G.L., Liquid-migration based model for predicting the thermal performance of spiral wound heat exchanger for floating LNG. Applied Energy, 2017, 206: 972–982.

[20] Duan Z.D., Ren T., Ding G.L., A dynamic model for FLNG spiral wound heat exchanger with multiple phase-change streams based on moving boundary method. Journal of Natural Gas Science and Engineering. 2016, 34: 657–669.

[21] Han H., Wang S.W., He T., et al. Numerical study of the falling film thickness around the tube bundle with different spacings between spray holes and tubes under tilt and sloshing conditions. International Journal of Heat and Mass Transfer, 2019, 138C: 184–193.

[22] Wang T., Ding G., Ren T., Chen J., Pu H., A mathematical model of floating LNG spiral-wound heat exchangers under rolling conditions. Applied Thermal Engineering 2016, 99: 959–969.

[23] Li S.L., Cai W.H., Chen J., et al., Evaluation analysis of correlations for predicting void fraction of condensation hydrocarbon refrigerant upward flow in a spiral pipe. Applied Thermal Engineering, 2018, 140: 716–732.

[24] Li S.L., Cai W.H., Chen J., et al., Numerical study on condensation heat transfer and pressure drop characteristics of ethane/propane mixture upward flow in a spiral pipe. International Journal of Heat and Mass Transfer, 2018, 121: 170–186.

[25] Li S.L., Jiang Y.Q., Cai W.H., et al., The influence of structural parameters on heat transfer and pressure drop for hydrocarbon mixture refrigerant during condensation in enhanced spiral pipes. Applied Thermal Engineering, 2018, 140: 759–774.

[26] Li S.L., Jiang Y.Q., Cai W.H., et al., Numerical study on condensation heat transfer and pressure drop characteristics of methane upward flow in a spiral pipe under sloshing condition. International Journal of Heat and Mass Transfer, 2019, 129: 310–325.

[27] Li S.L., Cai W.H., Jiang Y.Q., et al., The pressure drop and heat transfer characteristics of condensation flow with hydrocarbon mixtures in a spiral pipe under static and heaving conditions. International Journal of Refrigeration, 2019, 103: 16-31.

[28] Yu S.C., Chen J., Mi X.G., Lu L.Y., Experimental and numerical investigation of two-phase flow outside tube bundle of liquefied natural gas spiral wound heat exchangers under offshore conditions. Applied Thermal Engineering, 2019, 152: 103–112.

[29] Ren Y., Cai W., Chen J., Lu L., Wang J., Jiang Y., The heat transfer characteristic of shell-side film flow in spiral wound heat exchanger under rolling working conditions. Applied Thermal Engineering 2018, 132: 233–244.

[30] Ren Y., Cai W., Chen J., Lu L., Jiang Y., Numerical study on the shell-side flow and heat transfer of superheated vapor flow in spiral wound heat exchanger under rolling working conditions. International Journal of Heat and Mass Transfer 2018, 121: 691–702.

[31] Oka E., Heat exchanger design handbook. Petroleum Industry Press, Beijing, 1982.

[32] Bell K.J., Ghaly M.A., An approximate generalized design method for multicomponent/partial condenser. AIChE Symposium Series 1973, 69 (131): 72–79.

[33] Sun C.Z., Li Y.X., Han H., et al., Optimal selection of two-phase tube-side heat transfer model for small-scale LNG spiral wound heat exchanger. Chemical Industry Chemical Engineering Quarterly. 2019, 25 (1): 47–55.

[34] Sun C.Z., Li Y.X., Han H., et al., Experimental research on the adaptability of liquid natural gas spiral wound heat exchanger in dual mixed refrigeration liquefaction process. Experimental Thermal & Fluid Science, 2018, 98: 124–136.